

Revealing Quadrupolar Excitations with Nonlinear Spectroscopy

Yoshito Watanabe¹, Simon Trebst¹, and Ciarán Hickey^{2,3}

¹*Institute for Theoretical Physics, University of Cologne, 50937 Cologne, Germany*

²*School of Physics, University College Dublin, Belfield, Dublin 4, Ireland*

³*Centre for Quantum Engineering, Science, and Technology, University College Dublin, Dublin 4, Ireland*

 (Received 6 June 2024; revised 20 December 2024; accepted 24 February 2025; published 14 March 2025)

Local moments with a spin $S > 1/2$ can exhibit a rich variety of elementary quasiparticle excitations, such as quadrupolar excitations, that go beyond the dipolar magnons of conventional spin-1/2 systems. However, the experimental observation of such quadrupolar excitations is often challenging due to the dipolar selection rules of many linear response probes, rendering them invisible. Here we show that nonlinear spectroscopy, in the form of two-dimensional coherent spectroscopy (2DCS), can be used to reveal quadrupolar excitations. Considering a family of spin-1 Heisenberg ferromagnets with single-ion easy-axis anisotropy as an example, we explicitly calculate their 2DCS signature by combining exact diagonalization and generalized spin wave theory. We further demonstrate that 2DCS can provide access to the quadrupolar weight of an excitation, analogous to how linear response provides access to the dipolar weight. Our work highlights the potential of nonlinear spectroscopy as a powerful tool to diagnose multipolar excitations in quantum magnets.

DOI: [10.1103/PhysRevLett.134.106703](https://doi.org/10.1103/PhysRevLett.134.106703)

Quantum magnets admit a veritable zoo of distinct quasiparticle excitations, offering a versatile playground for the investigation of a diverse array of physics and phenomena. Alongside conventional dipolar excitations, such as the well-known magnons of spin-1/2 magnets, there is growing interest in the study of elementary excitations with *multipolar* character [1–3]. Such excitations arise in higher-spin magnets, or those with a more complex doublet structure, and greatly enrich the landscape of quasiparticle physics. As an example, in spin-1 systems, a purely on-site quadrupolar $|\Delta M^z| = 2$ excitation is possible as an elementary excitation, usually referred to as a single-ion bound state (SIBS) [4], whereas in spin-1/2 systems, a $|\Delta M^z| = 2$ excitation will necessarily only appear as a composite excitation, consisting of two dipolar excitations. Understanding the interplay of such excitations can provide deeper insights into fundamental phenomena like quasiparticle decay and renormalization [5].

Experimentally, studying multipolar excitations is hampered by the fact that they cannot be straightforwardly probed via linear response, which typically exhibits dipolar selection rules. However, there has been some recent progress [6,7] in revealing quadrupolar excitations under certain conditions: Although purely quadrupolar excitations cannot be created by a dipole operator, weakly breaking spin-rotational symmetry can hybridize quadrupolar and dipolar excitations, allowing both to appear even in conventional probes that follow dipolar selection rules. An alternative approach, which does not rely on such hybridization, involves using a probe that can couple with quadrupolar operators via local higher-order processes.

This latter approach has been demonstrated with RIXS spectroscopy [8].

Here, we show that one can straightforwardly access multipolar excitations via *nonlinear* response, encoded in a system's nonlinear susceptibilities and expressed in terms of higher-order dynamical correlation functions. As an example, for a spin-1 magnet with local moment at site i in the $|+1\rangle$ state, the third-order response can naturally encode elementary quadrupolar excitations via the matrix element $\langle +1|S_i^+|0\rangle\langle 0|S_i^+|-1\rangle\langle -1|S_i^-|0\rangle\langle 0|S_i^-|+1\rangle$. In general, the n th order response involves $n + 1$ spin operators, enabling the observation of $\Delta M^z = (n + 1)/2$ excitations for n odd.

An ideal technique for probing the nonlinear response of quantum magnets is two-dimensional coherent spectroscopy (2DCS). Using two THz field pulses separated by a time delay τ , one measures the magnetization a measurement time t after the second pulse. The technique can extract the second-order susceptibility $\chi^{(2)}(\omega_t, \omega_\tau)$, as well as two types of third-order susceptibilities: $\chi^{(3;1)}(\omega_t, \omega_\tau)$ and $\chi^{(3;2)}(\omega_t, \omega_\tau)$. There is a significant amount of ongoing research, from both experiment and theory, in trying to better understand THz 2DCS in magnetic materials [9–27].

In particular, we establish how 2DCS can reveal quadrupolar excitations, using a spin-1 ferromagnetic Heisenberg model with single-ion anisotropy as an example case study. Using a combination of exact diagonalization (ED) and linear generalized spin-wave theory (GSWT), we show that the energy of the SIBS can be measured by the third-order nonlinear susceptibility, $\chi_{xxxx}^{(3;1)}(\omega_t, \omega_\tau)$. Furthermore, we show that the other

third-order nonlinear susceptibility, $\chi_{xxxx}^{(3;2)}(\omega_l, \omega_r)$, can provide a measure of the quadrupolar weight of an excitation, even in cases with finite hybridization between dipolar and quadrupolar excitations, information not discernible from linear response alone.

Model and its excitations—As a paradigmatic example, we study the spin-1 ferromagnetic Heisenberg model with single-ion anisotropy on a regular d -dimensional lattice,

$$H = -J \sum_{\langle i,j \rangle} \mathbf{S}_i \cdot \mathbf{S}_j - D \sum_i (S_i^z)^2, \quad (1)$$

where $J > 0$ is the ferromagnetic Heisenberg coupling and $D > 0$ the single-ion anisotropy [4,28]. The model has a $U(1) \times \mathbb{Z}_2$ symmetry and the ground state, for $D/J > 0$, is a fully polarized ferromagnet along the z axis, $|\Psi_0^\pm\rangle = |\pm 1\rangle^{\otimes N}$, spontaneously breaking the discrete \mathbb{Z}_2 symmetry.

The $U(1)$ symmetry allows us to divide the Hilbert space into sectors with fixed $M^z = \sum_i S_i^z$. Since the application of $M^x \equiv \sum_i S_i^x$ can only change M^z by ± 1 , focusing solely on the $M^z = N, N-1, N-2$ sectors is sufficient when considering zero-temperature 2DCS. Combined with translational symmetry, the dimension of the Hilbert space to be considered is thus $\mathcal{O}(N)$, enabling us to evaluate nonlinear response using ED up to relatively large system sizes of $\mathcal{O}(100)$ sites (see Ref. [29] for details on the ED approach to 2DCS).

The energy spectrum at zero momentum, and its various excitations, calculated from ED for such a spin-1 ferromagnet is shown in Fig. 1. The simplest elementary excitation is a single magnon, a dipolar $|\Delta M^z| = 1$ excitation created by applying M^x to the fully polarized ground state. It has an energy $\omega_{1m} = D$ relative to the ground state. Above this, there is a continuum of 2-magnon states, spanning an energy range $2D \leq \omega_{2m} \leq 2D + 4zJ$, with z the coordination number of the lattice. These are $|\Delta M^z| = 2$ composite excitations which consist of pairs of dipolar single magnon excitations. Schematically, for, say, the $|\Psi_0^+\rangle$ ground state, the 1-magnon and 2-magnon excitations can be understood as flipping $|+1\rangle_i \rightarrow |0\rangle_i$ on a single site and flipping $|+1\rangle_i |+1\rangle_j \rightarrow |0\rangle_i |0\rangle_j$ on two different sites, respectively.

Crucially, for the $S = 1$ model, there is an additional elementary excitation with an intrinsic multipolar character. This is the SIBS [4], which, in the limit $D/J \rightarrow \infty$, can be understood as a full $|\Delta M^z| = 2$ spin flip on a single site, e.g., $|+1\rangle_i \rightarrow |-1\rangle_i$. In this limit, the energy of the SIBS $\omega_{\text{SIBS}} \rightarrow 2zJ$. Note that such an on-site quadrupolar excitation cannot occur in a purely spin-1/2 system, and is furthermore completely absent in linear response, which is only sensitive to dipolar excitations. At *finite* D/J it is important to realize that the nature of the SIBS is no longer as simple as the schematic $|+1\rangle_i \rightarrow |-1\rangle_i$ full spin flip presented in Fig. 1(b) (such a simple excited state is not

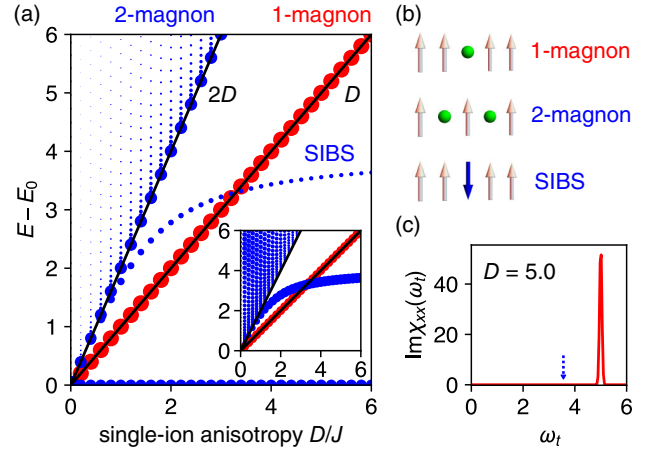


FIG. 1. Invisibility of quadrupolar excitation in linear response. (a) The energy spectrum, at zero momentum, of the spin-1 FM Heisenberg model with single-ion anisotropy D exhibits a 1-magnon excitation, a continuum of 2-magnon excitations, and a sharp single-ion bound state (SIBS). The size of the circles is proportional to the transition amplitudes $|\langle n|M^x|0\rangle|^2$ (red) and $|\langle n|(M^x)^2|0\rangle|^2$ (blue), with $n = 0, 1, \dots$ corresponding to the ground and excited states. Blue circles in the inset indicate $|\langle n|Q^{x^2-y^2}|0\rangle|^2$. As a representative example, the spectrum shown here is for a 1D $L = 100$ site chain. (b) Illustration of the schematic form of the various excitations. (c) Linear response at large $D = 5.0$ reveals only the 1-magnon excitation, while the quadrupolar SIBS is completely invisible.

even an eigenstate of the Hamiltonian due to the XY exchange terms contained within the Heisenberg interactions). We can dissect its true character by expanding $(M^x)^2$ as

$$(M^x)^2 = \frac{1}{2} \sum_i Q_i^{x^2-y^2} + \frac{1}{2} \sum_i (S_i^+ S_{i+1}^+ + S_i^- S_{i+1}^-) + \frac{1}{4} \sum_{i \neq j, j+1} (S_i^+ S_j^+ + S_i^- S_j^-) + \dots, \quad (2)$$

where the first term represents a purely on-site quadrupolar excitation (unique to spin-1 systems), the second represents a 2-magnon bound state (two magnons bound on neighboring sites), the third a regular 2-magnon state, and the ellipses $|\Delta M^z| = 0$ terms which do not play a role for the SIBS at the moment. Taking $D/J = 5$ in the 1-d chain as an example, the largest contribution for the SIBS comes from the first term, $\sim 65\%$ of the total weight, while the second and third terms contribute $\sim 30\%$ and $\sim 5\%$ respectively (see Supplemental Material [30] for D/J dependence). On the other hand, the lowest energy state in the 2-magnon continuum is fully dominated by the third term, $\sim 99\%$, which creates two magnons on two different sites. Thus, though the SIBS and 2-magnon states are both quadrupolar excitations, they have a fundamentally distinct underlying nature. The SIBS is a single, sharp elementary excitation

while the 2-magnon states form a continuum, and the SIBS has primarily on-site quadrupolar character while the 2-magnon states are composed of pairs of 1-magnon excitations. At small enough D/J , the SIBS merges with the 2-magnon continuum and loses its distinct nature.

2DCS quadrupolar signatures—Having understood the structure of the excitation spectrum, we now turn to how 2DCS can be used to reveal the presence of the SIBS. We focus on the third-order diagonal susceptibility $\chi_{xxxx}^{(3)}(t_3, t_2, t_1)$ (the second-order diagonal susceptibility vanishes). In the two-pulse setup used for 2DCS, there are two distinct contributions, $\chi_{xxxx}^{(3)}(t, \tau, 0)$ and $\chi_{xxxx}^{(3;2)}(t, 0, \tau)$. For now, we focus on the Fourier transformed $\chi_{xxxx}^{(3;1)}(\omega_t, \omega_\tau)$, which corresponds to two field interactions at time $t' = 0$ and one at $t' = \tau$.

As a useful comparison, we first consider a spin-1/2 XXZ model with longitudinal field, with Hamiltonian $H = -J \sum_{\langle i,j \rangle} [\gamma(S_i^x S_j^x + S_i^y S_j^y) + S_i^z S_j^z] - h_z \sum_i S_i^z$, and $\gamma/J = 1.1, h_z/J = 5.0$. The ground state is also a fully polarized ferromagnet along the z axis, with a 1-magnon excitation with energy $\omega_{1m} \approx h_z$ and a 2-magnon continuum for $\omega_{2m} \geq 2\omega_{1m}$ [Fig. 2(a)]. As shown in Fig. 2(c), in the 2DCS spectrum, there is a pump-probe (PP) peak at $(\omega_t, \omega_\tau) = (\omega_{1m}, 0)$ due to the 1-magnon excitation [9]. In addition, the lower edge of the 2-magnon continuum is visible as a 2Q peak at $(\omega_{1m}, 2\omega_{1m})$ [9].

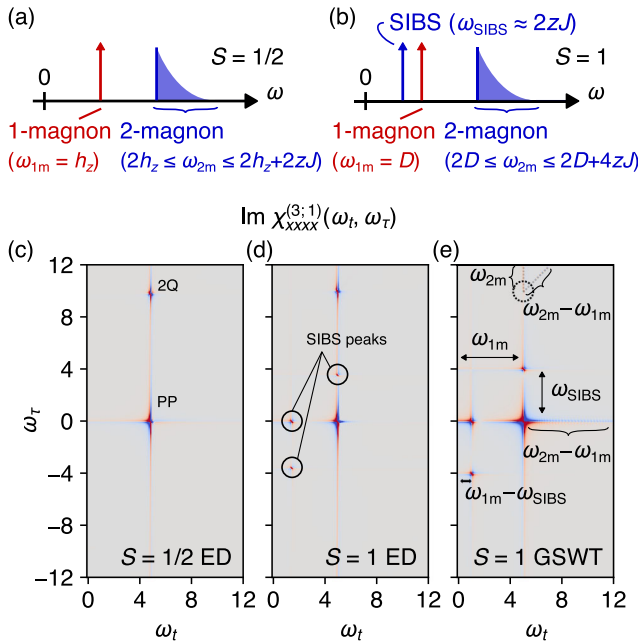


FIG. 2. 2DCS signatures of quadrupolar excitations. Schematics of excitation energies for (a) spin-1/2 FM XXZ model with longitudinal field and (b) spin-1 FM Heisenberg model with single-ion anisotropy in the large- D limit. Third-order susceptibility, $\chi_{xxxx}^{(3;1)}$, for $L = 100$ chain, calculated using ED for (c) spin-1/2 model and (d) spin-1 model at $D/J = 5.0$, with linear GSWT results in (e).

Now we consider our $S = 1$ model with $D/J \gg 1$. In this limit, the SIBS is well separated from both the 1-magnon excitation and the 2-magnon continuum [Fig. 2(b)]. In the 2DCS spectrum, we again observe the same PP and 2Q peaks from the 1-magnon excitation and 2-magnon continuum, respectively, just as in the spin-1/2 model. However, $\chi_{xxxx}^{(3;1)}$ now also contains *three additional peaks*, roughly located at $(\omega_{1m}, \omega_{\text{SIBS}})$, $(\omega_{1m} - \omega_{\text{SIBS}}, \omega_{\text{SIBS}})$, and $(\omega_{1m} - \omega_{\text{SIBS}}, 0)$. These additional peaks reveal quadrupolar excitation processes as can be intuitively understood, for instance, for the first of these peaks as follows: at time $t' = 0$, the two field interactions generate a SIBS excitation with energy ω_{SIBS} via $M^x(0)M^x(0)$. The system then evolves for a time τ , generating a peak at $\omega_\tau = \omega_{\text{SIBS}}$. At time $t' = \tau$, the single field interaction demotes the SIBS to a single magnon excitation via $M^x(\tau)$, which, after the system evolves for a time t , generates a peak at $\omega_t = \omega_{1m}$. Finally, at time $t' = t + \tau$, the system returns to the ground state via $M^x(t + \tau)$.

A more intuitive understanding of the 2DCS spectra can be obtained by comparing the numerical ED calculations with the linear GSWT approach [2], which treats magnon and quadrupolar excitations on equal footing. In GSWT, the Hamiltonian can be re-expressed using an SU(3) Schwinger boson $(\beta_{i,+1}, \beta_{i,0}, \beta_{i,-1})$ representation. In the FM case, the exact ground state, which we take here to be the fully polarized state $|\Psi_0^+\rangle = |+\rangle^{\otimes N}$, can be considered as a condensation of the $\beta_{i,+1}$ bosons. The remaining two flavors of bosons, $\beta_{i,0}$ and $\beta_{i,-1}$ correspond to $|0\rangle_i$ and $|-\rangle_i$ on-site excitations, which can then be used to represent the $\beta_{i,+1}$ operator as $\beta_{i,+1}^\dagger = \beta_{i,+1} = (1 - \beta_{i,0}^\dagger \beta_{i,0} - \beta_{i,-1}^\dagger \beta_{i,-1})^{1/2}$. Expanding the square root to quadratic order in $\beta_{i,0}, \beta_{i,-1}$, and inserting these into Eq. (1), we obtain the linear GSWT Hamiltonian in momentum space, for a lattice with a single-site unit cell, as

$$H_{\text{GSWT}} = \sum_k \omega_k \beta_{k,0}^\dagger \beta_{k,0} + 4J \sum_k \beta_{k,1}^\dagger \beta_{k,1}, \quad (3)$$

where $\omega_k = zJ + D - J\gamma_{\mathbf{k}}$, with $\gamma_{\mathbf{k}} = \sum_{\delta} e^{i\mathbf{k} \cdot \mathbf{e}_\delta}$ and \mathbf{e}_δ the z nearest-neighbor vectors. At $k = 0$, the energies of the 1-magnon and 2-magnon states are identical to the numerical ED results. On the other hand, the energy of the SIBS ω_{SIBS} is given as exactly $4J$, which agrees with the ED only in the limit $D/J \gg 1$. The inclusion of higher-order terms in the expansion of the square root is thus necessary to obtain the correct energy of the SIBS at smaller D/J . Indeed, the XY exchange part of the Hamiltonian produces a quartic term proportional to M^0 which, following a mean-field decomposition, will result in a correction to the SIBS dispersion. Using the GSWT approach, we can calculate the third-order susceptibility $\chi_{xxxx}^{(3)}(t, \tau, 0)$ in the time domain using

$$\begin{aligned} \chi_{xxxx}^{(3)}(t, \tau, 0) = & -\frac{1}{N} \sum_{PQR} A_{PQR} [2 \sin(\Delta E_{PR}\tau + \Delta E_{PQ}t) \\ & + \sin(-E_Q\tau + \Delta E_{PQ}t) \\ & + \sin(E_Q\tau + E_Rt)], \end{aligned} \quad (4)$$

where we have defined $\Delta E_{nm} = E_n - E_m$ (for simplicity we have set $E_0 = 0$), and $A_{PQR} = \langle 0|M^x|P\rangle\langle P|M^x|Q\rangle\langle Q|M^x|R\rangle\langle R|M^x|0\rangle$ is the transition amplitude. The result, shown in Fig. 2(d), demonstrates that, apart from the 2Q peak, the GSWT calculations successfully reproduce all of the qualitative features of the ED results. Indeed, all three peaks unique to the spin-1 model are confirmed to originate from processes in which the intermediate state $|Q\rangle$ is the SIBS $\beta_{k=0,-1}^\dagger|\text{vac}\rangle$. Not only does the GSWT approach provide insights into the origins of the various peaks, but much more importantly it can also be straightforwardly applied to other magnetically ordered states.

Evolution of excitations—So far, we have focused on the limit $D/J \gg 1$. Let us now consider what happens to the 2DCS spectrum as we lower the value of D/J . As D/J decreases, both ω_{1m} and ω_{SIBS} decrease, with their relative difference $\omega_{1m} - \omega_{\text{SIBS}}$ changing sign at, e.g., for the 1D chain, $D \approx 3$ (see Supplemental Material [30] for 2D and 3D cases). Consequently, the 2DCS peaks move within the 2D frequency plane, as indicated by the arrows in Figs. 3(b) and 3(c). Further decreasing D/J brings ω_{SIBS} close to the lower edge of the 2-magnon continuum, and mixing

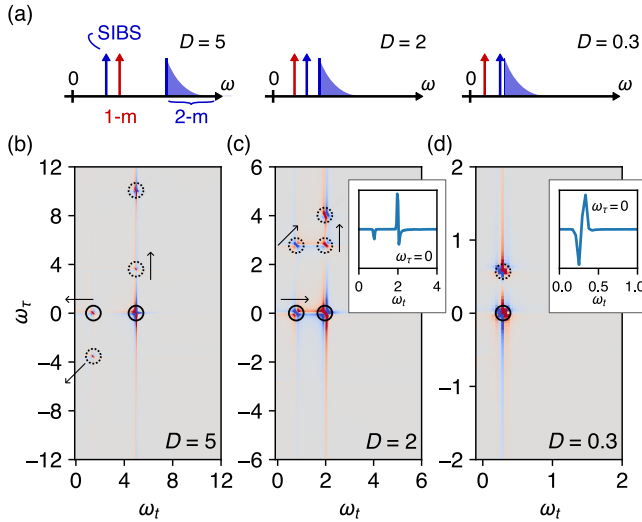


FIG. 3. Evolution of excitations. (a) The relative positions of the 1-magnon, SIBS, and 2-magnon continuum shift as D/J decreases. (b)–(d) $\chi_{xxxx}^{(3,1)}(\omega_t, \omega_\tau)$ for different D/J values, obtained by ED for an $L = 100$ chain. Arrows near the three SIBS peaks show the directions these peaks move towards the reference points at $(\omega_{1m}, 0)$ and $(\omega_{1m}, 2\omega_{1m})$. All peaks highlighted with solid/dotted circles eventually merge at small D/J . Insets display the line cut at $\omega_\tau = 0$.

between the states results in the SIBS acquiring dominant 2-magnon character. In this limit, the 2DCS spectrum now resembles that of the spin-1/2 model, in which only PP and 2Q peaks are visible [Fig. 3(d)]. However, as the PP peak consists of contributions from both the SIBS and the 1-magnon, an $\omega_\tau = 0$ line cut reveals a sign change at approximately $\omega_t \approx \omega_{1m} \approx \omega_{\text{SIBS}} - \omega_{1m}$ (insets of Fig. 3).

Note that the small D/J regime is of direct relevance to the material NiNb_2O_6 , considered to be an experimental realization of a spin-1 chain with easy-axis single-ion anisotropy [31]. There, the ratio D/J is estimated to be around 0.3 [31], which would put the material into the regime described above in which the SIBS has a strong 2-magnon character and the unique spin-1 peaks cannot be easily discerned [Fig. 3(d)].

Quadrupolar weight—In low symmetry models, in which the SIBS can hybridize with 1-magnon, the resulting hybridized mode can already be observed with conventional linear response probes such as neutron scattering [2,6,7]. As an example, consider the effect of a tilted magnetic field, $-h_z \sum_i S_i^z - h_y \sum_i S_i^y$, on our FM spin-1 Heisenberg model [30]. The transverse field h_y breaks the $U(1)$ symmetry of the model and thereby hybridizes the SIBS and the 1-magnon excitation, generating two modes, $|\psi_1\rangle$ and $|\psi_2\rangle$, which are both visible within linear response (the longitudinal field h_z is simply added to prevent, for the 1-d chain, the creation of free propagating domain walls on either side of the SIBS). The intensity of the linear response peaks, given by the matrix element $|\langle \psi_n | M^x | 0 \rangle|^2$ and shown in Fig. 4(a), is a measure of the dipolar weight of the excitations. We fix $D/J = 6$ such that, in the limit $h_y \rightarrow 0$, the modes $|\psi_1\rangle$ and $|\psi_2\rangle$ smoothly connect to the SIBS and 1-magnon excitation, respectively.

We can now use 2DCS to obtain additional information on the nature of the hybridized excitations, not accessible within linear response. To do so, we utilize the other third-order susceptibility $\chi_{xxxx}^{(3,2)}(\omega_t, \omega_\tau) \equiv \text{FT}[\chi_{xxxx}^{(3)}(t, 0, \tau)]$. As shown in Fig. 4(b), the diagonal nonrephasing peaks of $|\psi_1\rangle$ and $|\psi_2\rangle$ are clearly visible, and the appearance of cross peaks points to the hybridized nature of the two excitations [32]. In addition, four peaks at $(\omega_t, \omega_\tau) = (\omega_2 - \omega_1, \pm\omega_1)$ and $(\omega_2 - \omega_1, \pm\omega_2)$ are observed. One can show that the intensities of these additional peaks are given by

$$\begin{aligned} I_{(\omega_2 - \omega_1, \pm\omega_1)} & \propto m_{01}^x m_{12}^x m_{21}^x m_{10}^x \approx \left| \langle \psi_2 | (M^x)^2 | 0 \rangle \right|^2, \\ I_{(\omega_2 - \omega_1, \pm\omega_2)} & \propto m_{02}^x m_{21}^x m_{12}^x m_{20}^x \approx \left| \langle \psi_1 | (M^x)^2 | 0 \rangle \right|^2, \end{aligned} \quad (5)$$

where $m_{nm}^x = \langle n | M^x | m \rangle$, and the last approximation is justified since m_{nm}^x for $n > 2$ is negligible and $m_{nn}^x = 0$. We numerically confirm that the deviation between the intensity $I_{(E_2 - E_1, \pm E_1)}$ and $|\langle \psi_2 | (M^x)^2 | 0 \rangle|^2$ is less than 10% for $h_x < 0.5$ (and similar for the other peak), with the deviation

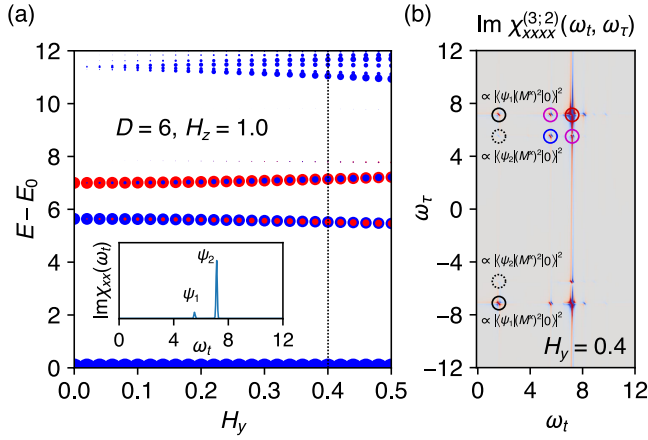


FIG. 4. Extracting quadrupolar weight of hybridized magnon and SIBS modes. (a) The evolution of the energy spectrum as a function of H_y , obtained by ED with $L = 12$. The size of circles are proportional to $|\langle n|M^x|0\rangle|$ (red) and $|\langle n|(M^x)^2|0\rangle|$ (blue). Inset shows the linear response at $H_y = 0.4$, where two modes $|\psi_1\rangle$ and $|\psi_2\rangle$ are visible due to the field-induced hybridization. (b) Third-order response $\chi_{xxxx}^{(3;2)}(\omega_t, \omega_\tau)$ at $H_y = 0.4$. In addition to diagonal peaks of $|\psi_1\rangle$ (blue), $|\psi_2\rangle$ (red), and off-diagonal peaks (pink, suggesting the hybridized nature of the two excitations), four peaks at $(\omega_t, \omega_\tau) = (E_2 - E_1, \pm E_1)$ and $(E_2 - E_1, \pm E_2)$ are observed. These peaks measure the quadrupolar weight of the modes.

largely due to contributions from higher excited states. Thus, the intensity of these 2DCS peaks can provide a measure of the quadrupolar weight of the excitations, $|\langle \psi_n | (M^x)^2 | 0 \rangle|^2$, analogous to how the intensity of the linear response peaks provides a measure of their dipolar weight, $|\langle \psi_n | M^x | 0 \rangle|^2$, allowing for a more sophisticated characterization of the quasiparticle spectrum. See Supplemental Material [30] for the comparison with the trivial hybridization between two 1-magnon modes.

Outlook—For various magnetic materials quadrupolar excitations have remained a theoretically expected but typically experimentally hidden feature, which 2DCS should now be able to clearly uncover. One material of much current interest is the easy-axis triangular magnet FeI_2 —another effective spin-1 magnet where the observation of a hybridized SIBS in neutron scattering experiment has been discussed in great detail [2,7]. Our work suggests that nonlinear spectroscopy could be used to directly probe the putative quadrupolar nature of these excitations, in particular, since for FeI_2 the SIBS is better separated from the 2-magnon continuum than for the NiNb_2O_6 chain compound mentioned previously. Along similar lines, one might reinspect other Ni^{2+} compounds [33] which may also show well-separated SIBS.

Outside of higher-spin magnets, another interesting class of materials expected to exhibit quadrupolar excitations are systems with non-Kramers doublets [34,35] whose local moments carry quadrupolar character. This includes the

rare-earth intermetallics $\text{Pr}(\text{Ti}, \text{V}, \text{Ir})_2(\text{Al}, \text{Zn})_{20}$ which exhibit quadrupolar-octupolar non-Kramers doublets [36,37] or $5d^2$ vacancy-ordered halide double perovskites [38]. As these systems lack any dipolar character, their excitations remain invisible in many conventional probes, but nonlinear 2DCS probes could be used to reveal their quadrupolar excitations [30].

In general, it should be clear that nonlinear response has enormous potential in probing multipolar excitations, both elementary multipolar excitations in $S > 1/2$ systems with easy-axis anisotropy or field-induced polarized phases [39,40] and non-Kramers doublets with multipolar character, as well as composite multipolar excitations such as exchange bound states, feasible even in spin-1/2 systems [21,41–46]. Though we focused here on a relatively simple spin-1 FM as a proof-of-concept example in this work, the linear GSWT approach can be straightforwardly extended to other ordered phases. However, to properly incorporate nonlinear corrections into GSWT, it is essential to renormalize the energies of one- and two-particle excitations on an equal footing. This ensures that the cancellation of different processes is accurately accounted for (see Supplemental Material [30] for more details). It can either be achieved through a mean-field approach or via direct numerical diagonalization [7]. In the latter case, it may be necessary to include subspaces beyond the two-particle subspace.

Acknowledgments—We thank A. Paramakanti for illuminating discussions. We acknowledge partial funding from the DFG within Project-ID 277146847, SFB 1238 (projects C02, C03). This work has benefitted from multiple exchanges during the 2023 KITP workshop “A New Spin on Quantum Magnets,” supported in part by Grant No. NSF PHY-1748958 to the Kavli Institute for Theoretical Physics (KITP). This work was performed in part at Aspen Center for Physics, which is supported by National Science Foundation Grant No. PHY-2210452. The numerical simulations were performed on the JUWELS cluster at the Forschungszentrum Juelich and the Noctua2 cluster at PC2 in Paderborn.

Data availability—The numerical data shown in the figures is available in Zenodo [47].

- [1] K. Penc, J. Romhányi, T. Rőom, U. Nagel, A. Antal, T. Fehér, A. Jánossy, H. Engelkamp, H. Murakawa, Y. Tokura, D. Szaller, S. Bordács, and I. Kézsmárki, Spin-stretching modes in anisotropic magnets: Spin-wave excitations in the multiferroic $\text{Ba}_2\text{CoGe}_2\text{O}_7$, *Phys. Rev. Lett.* **108**, 257203 (2012).
- [2] X. Bai, S.-S. Zhang, Z. Dun, H. Zhang, Q. Huang, H. Zhou, M. B. Stone, A. I. Kolesnikov, F. Ye, C. D. Batista, and M. Mourigal, Hybridized quadrupolar excitations in the

- spin-anisotropic frustrated magnet FeI_2 , *Nat. Phys.* **17**, 467 (2021).
- [3] K. Remund, R. Pohle, Y. Akagi, J. Romhányi, and N. Shannon, Semi-classical simulation of spin-1 magnets, *Phys. Rev. Res.* **4**, 033106 (2022).
- [4] R. Silberglitt and J. B. Torrance, Effect of single-ion anisotropy on two-spin-wave bound state in a Heisenberg ferromagnet, *Phys. Rev. B* **2**, 772 (1970).
- [5] M. E. Zhitomirsky and A. L. Chernyshev, Colloquium: Spontaneous magnon decays, *Rev. Mod. Phys.* **85**, 219 (2013).
- [6] A. Legros, S.-S. Zhang, X. Bai, H. Zhang, Z. Dun, W. A. Phelan, C. D. Batista, M. Mourigal, and N. P. Armitage, Observation of 4- and 6-magnon bound states in the spin-anisotropic frustrated antiferromagnet FeI_2 , *Phys. Rev. Lett.* **127**, 267201 (2021).
- [7] X. Bai, S.-S. Zhang, H. Zhang, Z. Dun, W. A. Phelan, V. O. Garlea, M. Mourigal, and C. D. Batista, Instabilities of heavy magnons in an anisotropic magnet, *Nat. Commun.* **14**, 4199 (2023).
- [8] A. Nag, A. Nocera, S. Agrestini, M. Garcia-Fernandez, A. C. Walters, S.-W. Cheong, S. Johnston, and K.-J. Zhou, Quadrupolar magnetic excitations in an isotropic spin-1 antiferromagnet, *Nat. Commun.* **13**, 2327 (2022).
- [9] J. Lu, X. Li, H. Y. Hwang, B. K. Ofori-Okai, T. Kurihara, T. Suemoto, and K. A. Nelson, Coherent two-dimensional terahertz magnetic resonance spectroscopy of collective spin waves, *Phys. Rev. Lett.* **118**, 207204 (2017).
- [10] Y. Wan and N. P. Armitage, Resolving continua of fractional excitations by spinon echo in THz 2D coherent spectroscopy, *Phys. Rev. Lett.* **122**, 257401 (2019).
- [11] S. A. Parameswaran and S. Gopalakrishnan, Asymptotically exact theory for nonlinear spectroscopy of random quantum magnets, *Phys. Rev. Lett.* **125**, 237601 (2020).
- [12] W. Choi, K. H. Lee, and Y. B. Kim, Theory of two-dimensional nonlinear spectroscopy for the Kitaev spin liquid, *Phys. Rev. Lett.* **124**, 117205 (2020).
- [13] Z.-L. Li, M. Oshikawa, and Y. Wan, Photon echo from lensing of fractional excitations in Tomonaga-Luttinger spin liquid, *Phys. Rev. X* **11**, 031035 (2021).
- [14] M. Fava, S. Biswas, S. Gopalakrishnan, R. Vasseur, and S. Parameswaran, Hydrodynamic nonlinear response of interacting integrable systems, *Proc. Natl. Acad. Sci. U.S.A.* **118**, e2106945118 (2021).
- [15] R. M. Nandkishore, W. Choi, and Y. B. Kim, Spectroscopic fingerprints of gapped quantum spin liquids, both conventional and fractonic, *Phys. Rev. Res.* **3**, 013254 (2021).
- [16] M. K. Negahdari and A. Langari, Nonlinear response of the Kitaev honeycomb lattice model in a weak magnetic field, *Phys. Rev. B* **107**, 134404 (2023).
- [17] O. Hart and R. Nandkishore, Extracting spinon self-energies from two-dimensional coherent spectroscopy, *Phys. Rev. B* **107**, 205143 (2023).
- [18] M. Fava, S. Gopalakrishnan, R. Vasseur, F. Essler, and S. A. Parameswaran, Divergent nonlinear response from quasiparticle interactions, *Phys. Rev. Lett.* **131**, 256505 (2023).
- [19] Y. Qiang, V. L. Quito, T. V. Trevisan, and P. P. Orth, Probing Majorana wavefunctions in Kitaev honeycomb spin liquids with second-order two-dimensional spectroscopy, *Phys. Rev. Lett.* **133**, 126505 (2024).
- [20] Q. Gao, Y. Liu, H. Liao, and Y. Wan, Two-dimensional coherent spectrum of interacting spinons from matrix product states, *Phys. Rev. B* **107**, 165121 (2023).
- [21] G. B. Sim, J. Knolle, and F. Pollmann, Nonlinear spectroscopy of bound states in perturbed Ising spin chains, *Phys. Rev. B* **107**, L100404 (2023).
- [22] G. B. Sim, F. Pollmann, and J. Knolle, Microscopic details of two-dimensional spectroscopy of one-dimensional quantum Ising magnets, *Phys. Rev. B* **108**, 134423 (2023).
- [23] Z. Zhang, F. Y. Gao, Y.-C. Chien, Z.-J. Liu, J. B. Curtis, E. R. Sung, X. Ma, W. Ren, S. Cao, P. Narang, A. von Hoegen, E. Baldini, and K. A. Nelson, Terahertz-field-driven magnon upconversion in an antiferromagnet, *Nat. Phys.* **20**, 788 (2024).
- [24] Z. Zhang, F. Y. Gao, J. B. Curtis, Z.-J. Liu, Y.-C. Chien, A. von Hoegen, M. T. Wong, T. Kurihara, T. Suemoto, P. Narang, E. Baldini, and K. A. Nelson, Terahertz field-induced nonlinear coupling of two magnon modes in an antiferromagnet, *Nat. Phys.* **20**, 801 (2024).
- [25] M. Potts, R. Moessner, and O. Benton, Exploiting polarization dependence in two-dimensional coherent spectroscopy: Examples of $\text{Ce}_2\text{Zr}_2\text{O}_7$ and $\text{Nd}_2\text{Zr}_2\text{O}_7$, *Phys. Rev. B* **109**, 104435 (2024).
- [26] M. McGinley, M. Fava, and S. A. Parameswaran, Signatures of fractional statistics in nonlinear pump-probe spectroscopy, *Phys. Rev. Lett.* **132**, 066702 (2024).
- [27] C. Huang, L. Luo, M. Mootz, J. Shang, P. Man, L. Su, I. E. Perakis, Y. X. Yao, A. Wu, and J. Wang, Extreme terahertz magnon multiplication induced by resonant magnetic pulse pairs, *Nat. Commun.* **15**, 3214 (2024).
- [28] N. Papanicolaou and G. C. Psaltakis, Bethe ansatz for two-magnon bound states in anisotropic magnetic chains of arbitrary spin, *Phys. Rev. B* **35**, 342 (1987).
- [29] Y. Watanabe, S. Trebst, and C. Hickey, Exploring two-dimensional coherent spectroscopy with exact diagonalization: Spinons and confinement in 1D quantum magnets, *Phys. Rev. B* **110**, 134443 (2024).
- [30] See Supplemental Material at <http://link.aps.org/supplemental/10.1103/PhysRevLett.134.106703> for full details of dipolar and quadrupolar operators, higher-dimensional FM spin-1 systems, impact of XXZ anisotropy, localized nature of SIBS, hybridized SIBS, hybridization of two dipolar magnon modes, generalized spin wave theory, and quadrupolar excitation in non-Kramers doublets.
- [31] P. Chauhan, F. Mahmood, H. J. Changlani, S. M. Koohpayeh, and N. P. Armitage, Tunable magnon interactions in a ferromagnetic spin-1 chain, *Phys. Rev. Lett.* **124**, 037203 (2020).
- [32] P. Hamm and M. Zanni, *Concepts and Methods of 2D Infrared Spectroscopy* (Cambridge University Press, Cambridge, England, 2011).
- [33] R. Koch, O. Waldmann, P. Müller, U. Reimann, and R. W. Saalfrank, Ferromagnetic coupling and magnetic anisotropy in molecular Ni(II) squares, *Phys. Rev. B* **67**, 094407 (2003).
- [34] S. B. Lee, S. Onoda, and L. Balents, Generic quantum spin ice, *Phys. Rev. B* **86**, 104412 (2012).

- [35] C. Liu, Y.-D. Li, and G. Chen, Selective measurements of intertwined multipolar orders: Non-Kramers doublets on a triangular lattice, *Phys. Rev. B* **98**, 045119 (2018).
- [36] A. Sakai and S. Nakatsuji, Kondo effects and multipolar order in the cubic $\text{PrTr}_2\text{Al}_{20}$ ($\text{Tr} = \text{Ti}, \text{V}$), *J. Phys. Soc. Jpn.* **80**, 063701 (2011).
- [37] F. Freyer, J. Attig, S. B. Lee, A. Paramekanti, S. Trebst, and Y. B. Kim, Two-stage multipolar ordering in $\text{PrT}_2\text{Al}_{20}$ Kondo materials, *Phys. Rev. B* **97**, 115111 (2018).
- [38] K. Pradhan, A. Paramekanti, and T. Saha-Dasgupta, Multipolar magnetism in $5d^2$ vacancy-ordered halide double perovskites, *Phys. Rev. B* **109**, 184416 (2024).
- [39] S. Zvyagin, C. Batista, J. Krzystek, V. Zapf, M. Jaime, A. Paduan-Filho, and J. Wosnitza, Observation of two-magnon bound states in the spin-1 anisotropic Heisenberg antiferromagnetic chain system $\text{NiCl}_2\text{-4SC(NH}_2)_2$, *Physica (Amsterdam)* **403B**, 1497 (2008).
- [40] M. Akaki, D. Yoshizawa, A. Okutani, T. Kida, J. Romhányi, K. Penc, and M. Hagiwara, Direct observation of spin-quadrupolar excitations in $\text{Sr}_2\text{CoGe}_2\text{O}_7$ by high-field electron spin resonance, *Phys. Rev. B* **96**, 214406 (2017).
- [41] R. Coldea, D. A. Tennant, E. M. Wheeler, E. Wawrzynska, D. Prabhakaran, M. Telling, K. Habicht, P. Smeibidl, and K. Kiefer, Quantum criticality in an Ising chain: Experimental evidence for emergent E_8 symmetry, *Science* **327**, 177 (2010).
- [42] Y. Nishida, Y. Kato, and C. D. Batista, Efimov effect in quantum magnets, *Nat. Phys.* **9**, 93 (2013).
- [43] C. M. Morris, R. Valdés Aguilar, A. Ghosh, S. M. Koohpayeh, J. Krizan, R. J. Cava, O. Tchernyshyov, T. M. McQueen, and N. P. Armitage, Hierarchy of bound states in the one-dimensional ferromagnetic Ising chain CoNb_2O_6 investigated by high-resolution time-domain terahertz spectroscopy, *Phys. Rev. Lett.* **112**, 137403 (2014).
- [44] B. Grenier, S. Petit, V. Simonet, E. Canévet, L.-P. Regnault, S. Raymond, B. Canals, C. Berthier, and P. Lejay, Longitudinal and transverse Zeeman ladders in the Ising-like chain antiferromagnet $\text{BaCo}_2\text{V}_2\text{O}_8$, *Phys. Rev. Lett.* **114**, 017201 (2015).
- [45] Z. Wang, J. Wu, W. Yang, A. K. Bera, D. Kamenskyi, A. T. M. N. Islam, S. Xu, J. M. Law, B. Lake, C. Wu, and A. Loidl, Experimental observation of Bethe strings, *Nature (London)* **554**, 219 (2018).
- [46] R. L. Dally, A. J. R. Heng, A. Keselman, M. M. Bordelon, M. B. Stone, L. Balents, and S. D. Wilson, Three-magnon bound state in the quasi-one-dimensional antiferromagnet $\alpha\text{-NaMnO}_2$, *Phys. Rev. Lett.* **124**, 197203 (2020).
- [47] Y. Watanabe, S. Trebst, and C. Hickey, Data underpinning “Revealing Quadrupolar Excitations with Non-Linear Spectroscopy,” [10.5281/zenodo.11106522](https://doi.org/10.5281/zenodo.11106522) (2024).